

Rotatable IRS Aided Wireless Communication

Qiaoyan Peng, *Graduated Student Member, IEEE*, Qingqing Wu, *Senior Member, IEEE*, Guangji Chen, Wen Chen, *Senior Member, IEEE*, Shaodan Ma, *Senior Member, IEEE*, Shanpu Shen, *Senior Member, IEEE*, Rui Zhang, *Fellow, IEEE*

Abstract—Rotatable intelligent reflecting surface (IRS) introduces a new spatial degree of freedom (DoF) by dynamically adjusting orientations without the need of changing its elements' positions in real time. To unleash the full potential of rotatable IRSs for wireless communications, this paper investigates the joint optimization of IRS rotation angles to maximize the minimum expected signal-to-noise ratio (SNR) over all locations within a given target area. We first propose an angle-dependent channel model that accurately characterizes the reception and reflection of each IRS element. Different from the conventional cosine-law assumption, the proposed model captures the practical electromagnetic characteristics of the IRS, including the effective reception area and reflection efficiency. For the single target location case, a particle swarm optimization (PSO)-based algorithm is developed to solve the SNR maximization problem, and a closed-form expression for a near-optimal solution is derived to provide useful insights. For the general area coverage enhancement case, the optimal rotation is obtained through a two-loop PSO-based iterative algorithm with null-point detection. In this algorithm, the outer loop updates the global rotation angles to maximize the minimum SNR over the target area, whereas the inner loop evaluates the SNR distribution within the area to identify the location corresponding to the minimum SNR through null-point detection. Numerical results demonstrate significant SNR improvement achieved by the proposed rotatable IRS design over various benchmark schemes under different system setups.

Index Terms—Intelligent reflecting surface (IRS), rotatable IRS, rotation optimization, particle swarm optimization (PSO), coverage enhancement.

I. INTRODUCTION

The development of the sixth-generation (6G) wireless networks is driven by the ambition to achieve unprecedented data rates, superior energy efficiency, and broader network coverage, which aim to support the demanding requirements of future ubiquitous connectivity [1]–[3]. As a promising solution, intelligent reflecting surfaces (IRSs) have been introduced as a cost- and energy-efficient complement to traditional wireless networks, offering proactive and flexible control of the radio-wave propagation. By dynamically adjusting the

amplitude and/or phase of passive elements, IRSs can reconfigure wireless channels to strengthen desired signals, suppress interference, improve physical-layer security, and extend network coverage in challenging propagation scenarios. These capabilities allow the IRS to support diverse applications such as interference mitigation in dense networks, throughput improvement for cell-edge users, and simultaneous wireless information and power transfer for energy-limited devices [4]–[6]. Motivated by these prospects, extensive research has been conducted on IRS-aided systems, focusing on main issues including energy efficiency maximization, joint active and passive beamforming design, and the theoretical analysis of achievable rate regions [7]–[10].

The aforementioned studies mainly consider IRSs that are installed at fixed locations with pre-determined orientations to enhance wireless communication systems. In existing works, the IRS is primarily deployed in terrestrial scenarios, where it is typically mounted on the outer walls of buildings, indoor ceilings, and other static structures [11]–[13]. As a fixed IRS can only provide effective service to transmitters and receivers located within the same half-space relative to its reflective surface, communication nodes positioned on the opposite sides of the IRS cannot benefit from its reflection capability, which restricts its spatial coverage. Moreover, although passive beamforming can be used to reflect signals toward users, each reflection may lead to partial scattering of the electromagnetic waves in undesired directions. This dispersion of signal energy results in additional propagation loss and severe attenuation, which significantly degrade the overall signal quality and reduce the efficiency of the IRS-aided links, especially in complex propagation environments.

To address the limitations of conventional fixed IRSs, recent research has explored dynamic deployment strategies that can operate in a more adaptive and flexible manner. These strategies introduce movable and rotatable IRS in wireless communication systems, thereby opening new opportunities for fully harnessing the potential of the IRS technology in next-generation wireless systems. To be specific, aerial IRS-enabled three-dimensional (3D) wireless networks, where the IRS is mounted on aerial platforms, e.g., unmanned aerial vehicles (UAVs), have received significant attention for intelligent signal reflection [14]–[17]. Different from traditional terrestrial IRSs, which are inherently restricted to serving only the nodes located within the same half-space of the reflective surface, an aerial IRS can achieve near-omnidirectional reflection and facilitate line-of-sight (LoS) communication between transmitters and receivers due to its elevated position relative to the ground. In [14], transmit beamforming, IRS placement, and 3D passive beamforming were jointly optimized to maximize

Q. Peng is with the Department of Electronic Engineering, Shanghai Jiao Tong University, Shanghai 200240, China, and also with the State Key Laboratory of Internet of Things for Smart City, University of Macau, Macao 999078, China (email: qiaoyan.peng@connect.um.edu.mo). Q. Wu and W. Chen are with the Department of Electronic Engineering, Shanghai Jiao Tong University, Shanghai 200240, China (email: qingqingwu@sjtu.edu.cn; wenchen@sjtu.edu.cn). G. Chen is with Nanjing University of Science and Technology, Nanjing 210094, China (email: guangjichen@njust.edu.cn). S. Ma and S. Shen are with the State Key Laboratory of Internet of Things for Smart City, University of Macau, Macao 999078, China (email: shaodanma@um.edu.mo; shanpushen@um.edu.mo). R. Zhang is with the Department of Electrical and Computer Engineering, National University of Singapore, Singapore 117583 (e-mail: elezhang@nus.edu.sg).

the worst-case signal-to-noise ratio (SNR) within a target area, utilizing a beam broadening and flattening technique to achieve significant performance gains over the fixed IRS. Furthermore, the maneuverability of UAVs allows the location and orientation of an aerial IRS to be dynamically adjusted, which introduces additional degrees of freedom for system optimization and enables highly flexible 3D network design that can adapt to real-time changes in communication demands. The work [15] developed an efficient alternating optimization algorithm in a UAV-mounted IRS-aided multicast system with the joint design of the IRS's 3D location, 3D orientation, and passive beamforming. Despite many advantages mentioned above, aerial IRS poses fundamental limitations for several reasons. First, the endurance, stability, and controllability of the aerial platform remain critical technical concerns, as the platform must support sustained operation under varying environmental conditions [18]. Second, platform drift and vibration, which influence reflection accuracy and system stability, as well as the complexity associated with optimizing the placement and trajectory of aerial platforms, impose significant design burdens [19]. Third, regulatory constraints related to flight zones and airspace management may further limit the large-scale or long-term deployment of aerial IRSs in practical scenarios [20].

Considering the ease of implementation provided by the fixed IRS and the high flexibility offered by the aerial IRS, the rotatable IRS has been proposed, which focuses on dynamic orientation adjustment rather than full spatial displacement [21]–[26]. To be specific, a rotatable IRS can flexibly vary its rotation angles at a fixed position, thereby dynamically reconfiguring its reception and reflection patterns and providing additional spatial degrees of freedom without physical movement. By properly adjusting its rotation angle, a single rotatable IRS can achieve panoramic coverage or full-angle reflection, enabling it to serve any transmitter-receiver pair within its coverage region. Moreover, the practical implementation of a rotatable IRS resembles existing rotatable antennas, where the IRS is mounted on a motor-driven shaft, and its rotation angles is precisely controlled through mechanical adjustment mechanisms, which can also be considered as a special case of the general six-dimensional movable antenna (6DMA) model with both 3D position and 3D orientation control [27]–[32]. Such an architecture ensures strong compatibility with existing wireless infrastructures while avoiding the need for continuous positioning, complex mechanical control, and the high power consumption typically associated with mobile platforms. Because of its simple structure, low energy cost, and low latency, a rotatable IRS is appealing for scenarios that require rapid adaptation but where large-scale mechanical movement is impractical. The rotatable IRS has been extensively investigated under various communication systems, including cellular systems [22], mobile edge computing systems [23], and multicast systems [24]. In [22], the received power was maximized when the incident angle was zero. The work [23] proposed a deep learning-based algorithm for the joint design of IRS orientation, phase shifts, and offloading strategies. The base station (BS) beamforming, IRS phase shifts, and orientation adjustment were jointly optimized

to maximize the multicast rates in [23].

Despite the effectiveness of the IRS rotation strategies, most existing studies have relied on a simplified and idealized channel model that primarily accounts for the propagation path loss and orientation parameters, while overlooking other crucial physical-layer characteristics such as the effective reception area of the IRS, as well as its reception and reflection efficiency [33]–[35]. Consequently, the corresponding deployment strategies may underperform in practical scenarios with non-ideal channels, as they fail to capture the geometric and physical constraints inherent in practical channel conditions [36]. To address this issue, the work [37] assumed an IRS with predetermined electromagnetic properties and focused on how its steering capability affects the spatial power redistribution of the reflected beam. Furthermore, a physics-based model was proposed in [38], where the IRS elements were grouped into tiles whose effects on the wireless channel were characterized by solving the electric and magnetic field integral equations. In the above studies, the IRS is represented as a continuous reflecting surface whose global response determines the scattered beam. It provides analytical simplicity and facilitates theoretical investigations. In contrast, the IRS can be modeled as a planar distribution of discrete controllable elements that capture the collective response produced by the individual reflecting elements, which provides a more accurate and practical framework for IRS design by capturing its physical characteristics. One of the main advantages lies in allowing the electromagnetic properties to be directly integrated with circuit-level models of the tunable elements, thereby bridging the gap between idealized analysis and practical design. In [39], the authors evaluated the scattering performance, power, and size of a single IRS element and then maximized the received signal power toward a specific user. Furthermore, the rotation of the IRS was optimized to maximize the worst SNR over all locations in a target area in both indoor [40] and outdoor scenarios [41]. However, in [39]–[41], the radiation patterns of the transmit and receive antennas, as well as the IRS elements, are modeled with angle-dependent factors derived from a simplified cosine law, which may lead to limitations of rotation optimization in terms of SNR.

Motivated by the above discussion, this paper investigates a rotatable IRS-aided wireless communication system, where the IRS is deployed to extend BS coverage toward a specific target area, e.g., a cellular hot spot or a remote zone lacking access. Specifically, we aim to design the IRS rotation to maximize the worst-case/minimum SNR in the target area, thereby improving the performance. The corresponding optimization problem is challenging to solve directly for the following reasons. First, in contrast to the cosine law-based model, a more practical channel model is required to capture the impact of the IRS rotation by characterizing the reception and reflection behaviors of each IRS element, which lays the foundation for further performance analysis. Since this elaborate model introduces additional spatial dependencies and nonlinear coupling into the problem formulation, it significantly increases the analytical complexity. Second, different from the conventional fixed IRS, the rotation of the rotatable IRS introduces a new set of design variables that influence not only the incident and reflection

angles at the IRS but also the angular extent from the IRS that covers the target area. These coupled effects determine the effective coverage range and directivity of the reflected beam, thereby significantly affecting the quality of the received signals. Third, compared with prior studies that steer the IRS beam toward a single user at a known location, the IRS rotation is optimized by taking into account all possible user positions within a given target area, which leads to a more complex and challenging optimization problem. The main contributions of this paper are summarized as follows:

- First, we study a rotatable IRS-aided wireless communication system by optimizing the rotation angles of the IRS. A practical angle-dependent channel model based on electromagnetic field modeling is proposed, which accounts for the reception and reflection factors. With the optimized BS and IRS beamforming for each user location, we derive the closed-form expression of the corresponding received SNR with respect to (w.r.t.) the IRS rotation angle. By utilizing the proposed model, we formulate an optimization problem aimed at maximizing the minimum SNR over all locations in the given area, subject to the rotation constraint to ensure effective reflection.
- Next, we consider the case of SNR maximization at a specific user location and propose an efficient particle swarm optimization (PSO)-based algorithm for the IRS rotation design. Given that the rotatable IRS is generally electrically small, we derive a closed-form expression for a near-optimal solution. Furthermore, the optimal elevation angle approaches $-\pi/2$ when the IRS is deployed at a sufficiently high altitude, which is independent of the azimuth angle. Moreover, no rotation is needed when both the BS and the user are far away from the IRS along the x -axis (see Fig. 1). For the general case of min-SNR maximization in a target area, we propose a PSO-based two-loop Iterative algorithm. To reduce the complexity, null point detection can be applied to avoid exhaustive search over all user locations.
- Finally, extensive numerical results are presented to validate our theoretical results and demonstrate the significant performance gains achieved by the rotatable IRS over other benchmark schemes under different setups. Moreover, it is shown that our proposed scheme achieves about 3 dB gain in SNR over conventional fixed IRS scheme for the special case of a single target location.

The remainder of this paper is organized as follows. Section II introduces the system model and formulates the optimization problem for the rotatable IRS-aided wireless communication system. Sections III and IV propose efficient algorithms for the single target location and area coverage scenarios, respectively. Section V provides numerical results that evaluate our proposed designs. Section VI concludes the paper.

Notations: Scalars are represented by italic letters. Vectors and matrices are denoted by bold lowercase and uppercase letters, respectively. The modulo operation $\text{mod}(a, b)$ returns the remainder of the division of a by b . For real number s , $\lfloor s \rfloor$ denotes the floor operation and $\text{sinc}(s) \triangleq \sin(s)/s$. For

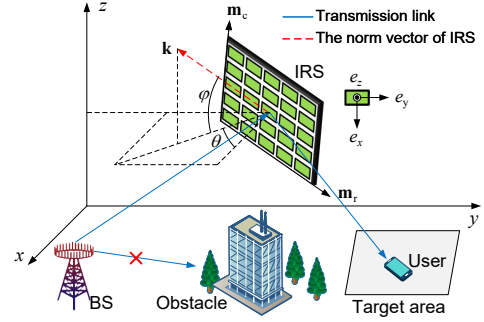


Fig. 1. A rotatable IRS-aided wireless communication system.

a vector \mathbf{s} , $\|\mathbf{s}\|$, and $[\mathbf{s}]_n$ denote its Euclidean norm and n -th entry, respectively. For a matrix \mathbf{S} , $[\mathbf{S}]_{m,n}$ denotes the element on the m -th row and n -th column of \mathbf{S} . j denotes the imaginary unit with $j^2 = -1$.

II. SYSTEM MODEL

As shown in Fig. 1, we consider an IRS-aided wireless communication system, where the IRS is deployed to assist from the multi-antenna BS to the single-antenna user within the target area \mathcal{A} . We focus on a challenging scenario where the direct BS-user link is blocked by obstacles and assume that all the considered channels follow the free-space LoS model [42], [43]. The IRS consists of a total of $N = N_c \times N_r$ elements, arranged in N_r rows and N_c columns, with each element have the size of $\bar{l} \times \bar{l}$. The BS is equipped with a conventional UPA placed on the x - y plane, and the total number of antennas is $M = M_c \times M_r$ antennas, where M_r and M_c denote the number of antennas along the x - and y -axis, respectively. In the considered system, we establish a global Cartesian coordinate system (CCS). Assuming that the target area \mathcal{A} is a rectangular area with length A_x and width A_y on the x - y plane, its center is denoted as $\mathbf{p}_r = [x_r, y_r, 0]^T$. Thus, any user location within the target area \mathcal{A} is located at $\mathbf{p}_U = [x_U, y_U, 0]^T$ with $x_U \in [x_r - A_x/2, x_r + A_x/2]$ and $y_U \in [y_r - A_y/2, y_r + A_y/2]$.

Let $\boldsymbol{\Omega} = (\theta, \phi)^T$ denote the rotation angles of the IRS, where θ and ϕ are the azimuth and elevation angles, respectively, within the feasible set $\mathcal{S} = \{(\theta, \phi)^T | \theta \in [-\pi/2, \pi/2], \phi \in [-\pi/2, \pi/2]\}$. Thus, the normal vector of the IRS is expressed as

$$\mathbf{k} = (\cos \theta \cos \phi, -\sin \theta \cos \phi, \sin \phi)^T. \quad (1)$$

The reflecting elements of the IRS are placed on lines along two orthogonal base directions, which are given by

$$\mathbf{m}_c = (-\cos \theta \sin \phi, \sin \theta \sin \phi, \cos \phi)^T, \quad (2)$$

$$\mathbf{m}_r = (\sin \theta, \cos \theta, 0)^T. \quad (3)$$

In the initial stage, the IRS is set without rotation, i.e., $\theta = 0$ and $\phi = 0$. As such, we have $\mathbf{k} = (1, 0, 0)^T$, $\mathbf{m}_r = (0, 1, 0)^T$ and $\mathbf{m}_c = (0, 0, 1)^T$, which are the unit vectors along the x -, y -, and z -axis of the global CCS, respectively.

As illustrated in Fig. 2, without loss of generality, the IRS reflecting elements are assumed to be arranged in a rectangular

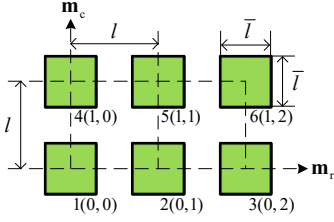


Fig. 2. An example of a rectangular IRS with 6 elements, where each reflecting element in a specific row and a specific column is labeled with a unique index.

array. The elements are arranged along lines in the two base directions, i.e., \mathbf{m}_r and \mathbf{m}_c , with an inter-element spacing of l in each direction. We map the reflecting element located at N_n^r -th row and N_n^c -th column as the n -th element of the IRS, with $N_n^r \in \mathcal{N}_r = \{0, \dots, N_r - 1\}$, $N_n^c \in \mathcal{N}_c = \{0, \dots, N_c - 1\}$, and $n \in \mathcal{N} = \{1, \dots, N\}$, where

$$N_n^r = \lfloor (n - 1) / N_c \rfloor, n \in \mathcal{N}, \quad (4)$$

$$N_n^c = n - N_c N_n^r - 1, n \in \mathcal{N}. \quad (5)$$

The bottom-left element of the IRS is defined as the 1st element of the UPA whose coordinate is given by $\mathbf{p}_1 = [x_1, y_1, z_1]^T$. We take the 1st element of the IRS as the reference point. Accordingly, the coordinate for the n -th element of the IRS is expressed as

$$\mathbf{p}_n = \mathbf{p}_1 + N_n^c l \mathbf{m}_r + N_n^r l \mathbf{m}_c, n \in \mathcal{N}, \quad (6)$$

where l is the distance between two adjacent IRS elements. Then, the center coordinate for the IRS is expressed as

$$\mathbf{p}_c = \mathbf{p}_1 + \frac{N_c - 1}{2} l \mathbf{m}_r + \frac{N_r - 1}{2} l \mathbf{m}_c, n \in \mathcal{N}. \quad (7)$$

Similar to the IRS, we map the antenna located at M_m^r -th row and M_m^c -th column as the m -th antenna of the BS, with $M_m^r \in \mathcal{M}_r = \{0, \dots, M_r - 1\}$, $M_m^c \in \mathcal{M}_c = \{0, \dots, M_c - 1\}$, and $m \in \mathcal{M} = \{1, \dots, M\}$, where

$$M_m^r = \lfloor (m - 1) / M_c \rfloor, m \in \mathcal{M}, \quad (8)$$

$$M_m^c = m - M_c M_m^r - 1, m \in \mathcal{M}. \quad (9)$$

We denote the coordinates for the 1st antenna of the BS as $\mathbf{p}_{B,1} = [x_{B,1}, y_{B,1}, 0]^T$. Accordingly, the coordinate for the m -th antenna of the BS is given by

$$\mathbf{p}_{B,m} = \mathbf{p}_{B,1} + M_m^c \tilde{l} \mathbf{m}_B^c + M_m^r \tilde{l} \mathbf{m}_B^r, m \in \mathcal{M}. \quad (10)$$

where $\mathbf{m}_B^r = [0, 1, 0]^T$, $\mathbf{m}_B^c = [-1, 0, 0]^T$, and \tilde{l} is the distance between two adjacent BS antennas. Then, the center coordinate for the BS is expressed as

$$\mathbf{p}_B = \mathbf{p}_{B,1} + \frac{M_c - 1}{2} \tilde{l} \mathbf{m}_B^c + \frac{M_r - 1}{2} \tilde{l} \mathbf{m}_B^r. \quad (11)$$

The distance between the center of the BS and the center of the IRS, as well as the distance between the center of the IRS and any location of the target area $\mathbf{p}_U \in \mathcal{A}$ are given by

$$t = \|\mathbf{p}_B - \mathbf{p}_c\|, \quad r = \|\mathbf{p}_U - \mathbf{p}_c\|, \quad (12)$$

respectively. Under the LoS channel, the entry in column n of the channel from the IRS to the user, i.e., \mathbf{f}^H , is given by

$$[\mathbf{f}^H]_n = \frac{\sqrt{\beta}}{r_n} e^{-j \frac{2\pi}{\lambda} r_n}, n \in \mathcal{N}, \quad (13)$$

where $r_n = \|\mathbf{p}_U - \mathbf{p}_n\|$ is the distance between the user and the n -th element of the IRS, β is the channel power gain at the reference distance, i.e., 1 meter (m), and λ denotes the carrier wavelength.

The entry in row n and column m of the channel from the m -th antenna of the BS to the n -th element of the IRS, i.e., \mathbf{G} , is given by

$$[\mathbf{G}]_{n,m} = \frac{\sqrt{\beta}}{t_{n,m}} e^{-j \frac{2\pi}{\lambda} t_{n,m}}, n \in \mathcal{N}, m \in \mathcal{M}, \quad (14)$$

where $t_{n,m} = \|\mathbf{p}_{B,m} - \mathbf{p}_n\|$ is the distance from the m -th antenna of the BS to the n -th element of the IRS.

The received signal at the typical user within the target area is given by

$$y = \mathbf{f}^H \Phi \mathbf{G} \mathbf{w} s + n_0, \quad (15)$$

where the coefficient matrix of the IRS is $\Phi = \text{diag}(\eta_1, \dots, \eta_N)$ with the reflection coefficients $\eta_n, n \in \mathcal{N}$, $\mathbf{w} = [w_1, \dots, w_M]^T$ denotes the BS beamforming vector satisfying $\|\mathbf{w}\|^2 \leq P_t$, s stands for the symbol transmitted from BS with power P_t , $n_0 \sim \mathcal{CN}(0, \sigma_0^2)$ denotes the additive Gaussian white noise (AWGN) at the receiver with σ_0^2 representing the noise power.

We denote $\varpi_B^c = \arccos\left(\frac{(\mathbf{p}_{B,1} - \mathbf{p}_1) \cdot \mathbf{m}_B^c}{\|\mathbf{p}_{B,1} - \mathbf{p}_1\| \cdot \|\mathbf{m}_B^c\|}\right)$, $\varpi_B^r = \arccos\left(\frac{(\mathbf{p}_{B,1} - \mathbf{p}_1) \cdot \mathbf{m}_B^r}{\|\mathbf{p}_{B,1} - \mathbf{p}_1\| \cdot \|\mathbf{m}_B^r\|}\right)$, $\varpi_c = \arccos\left(\frac{(\mathbf{p}_{B,1} - \mathbf{p}_1) \cdot \mathbf{m}_c}{\|\mathbf{p}_{B,1} - \mathbf{p}_1\| \cdot \|\mathbf{m}_c\|}\right)$, and $\varpi_r = \arccos\left(\frac{(\mathbf{p}_{B,1} - \mathbf{p}_1) \cdot \mathbf{m}_r}{\|\mathbf{p}_{B,1} - \mathbf{p}_1\| \cdot \|\mathbf{m}_r\|}\right)$ as the angles between $(\mathbf{p}_{B,1} - \mathbf{p}_1)$ and \mathbf{m}_B^c , \mathbf{m}_B^r , \mathbf{m}_c , and \mathbf{m}_r , respectively. According to [11], the LoS channel from the BS to the IRS can be assumed to be a rank-one matrix if $t_{1,1} \geq \sqrt{N} \tilde{l} / \lambda$. To facilitate the design of the BS and IRS beamforming, we provide a tractable characterization for the BS-IRS channel in the following proposition.

Proposition 1: Under the assumption that $t_{1,1} \geq \sqrt{N} \tilde{l} / \lambda$, the BS-IRS channel entry can be approximated as

$$[\mathbf{G}]_{n,m} \approx \frac{\sqrt{\beta}}{t_{n,m}} e^{-j \frac{2\pi}{\lambda} (t_{1,1} + \bar{g}_m + \bar{g}_n)}, n \in \mathcal{N}, m \in \mathcal{M}, \quad (16)$$

where $\bar{g}_m = M_m^c \tilde{l} \cos \varpi_B^c + M_m^r \tilde{l} \cos \varpi_B^r$, $m \in \mathcal{M}$ and $\bar{g}_n = -N_n^c \tilde{l} \cos \varpi_c - N_n^r \tilde{l} \cos \varpi_r$, $n \in \mathcal{N}$.

Proof: Please refer to Appendix A. ■

According to Proposition 1, the channel matrix \mathbf{G} can be reformulated based on the geometric relationship between BS and IRS, and its phase is decomposed into a constant term, a term dependent on the BS antenna index, and a term dependent on the IRS element index.

Let θ_n^i , ϕ_n^i , θ_n^r , and ϕ_n^r denote the azimuth and elevation angles of the incident wave as well as the azimuth and elevation angles of the reflected wave relative to the n -element of the IRS, respectively. Different from the traditional signal-reflection model, we consider an angle-dependent signal

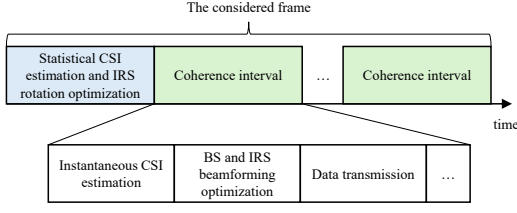


Fig. 3. Illustration of the two-timescale design.

reflection model based on electromagnetic-field modeling that takes into account the effective IRS reflection aperture, as represented in the following proposition.

Proposition 2: The reflection coefficient of the n -th IRS element is given by

$$\eta_n = \sqrt{\frac{4\pi\bar{l}^4}{\lambda^2}} \alpha_n \gamma_n e^{j\psi_n}, \quad (17)$$

where ψ_n denotes its phase shift. The reception factor and the reflection factor of the n -th IRS element are denoted by $\alpha_n = \cos\phi_n^i$, $\gamma_n = Z_n \text{sinc}(X_n) \text{sinc}(Y_n)$ with $X_n = \frac{\pi\bar{l}}{\lambda} (\sin\theta_n^i \cos\phi_n^i + \cos\theta_n^r \sin\phi_n^r)$, $Y_n = \frac{\pi\bar{l}}{\lambda} (\sin\theta_n^r \sin\phi_n^r - \sin\theta_n^i \sin\phi_n^i)$, and $Z_n = \sqrt{\cos^2\phi_n^r \sin^2(\phi_n^i + \theta_n^r) + \cos^2(\phi_n^i + \theta_n^r)}$.

Proof: Please refer to Appendix B. ■

It is observed from Proposition 2 that the reflection coefficient of each IRS element is based on a physical angle-dependent model which characterizes its inherent electromagnetic response by accounting for the reception factor, α_n , and the reflection factor, γ_n . Specifically, the reception factor α_n indicates the impact of the cosine of the incident azimuth angle on the energy-capturing capability of each element. Moreover, we observe that the reflection factor γ_n includes two sinc functions, both of which are fundamentally constrained by the element's wavelength-normalized length, i.e., \bar{l}/λ .

The received signal power is given by

$$P_r = \frac{4\pi\bar{l}^4\beta^2}{\lambda^2} \left| \sum_{m=1}^M e^{-j\frac{2\pi}{\lambda}\bar{g}_m} w_m \sum_{n=1}^N \frac{\alpha_n \gamma_n}{t_{n,m} r_n} e^{j(\varphi_n - \frac{2\pi}{\lambda}(\bar{g}_n + r_n))} \right|^2. \quad (18)$$

As such, the received SNR at the location $\mathbf{p}_U \in \mathcal{A}$ is given by $\varsigma = P_r/\sigma_0^2$.

As shown in Fig. 3, we propose a two-timescale design, where the short-term transmit beamforming at the BS \mathbf{w} , the short-term IRS reflection phase shifts Φ , and the long-term IRS rotation angles $\Omega = (\theta, \phi)^T$ are jointly optimized to maximize the worst-case/minimum SNR within the target \mathcal{A} . Specifically, the IRS rotation angles are first optimized based on the statistical channel state information (CSI), which depends on the angle and location information that typically remain unchanged over the long term. This is because the IRS rotation is realized through mechanical control, which varies over a large timescale. In contrast, the phase shifts of the IRS are adaptively adjusted for the typical user within the target area, since they can be updated rapidly through electronic control in response to user mobility. Then, the beamforming

vectors at both the BS and the IRS are designed based on the effective instantaneous CSI with the optimized IRS rotation obtained in the previous step. Our two-timescale design effectively reduces the update frequency of IRS rotation and allows the system to exploit fast beamforming reconfiguration and robust orientation, thereby ensuring reliable coverage and enhanced signal strength over the target region.

Given Φ and Ω , the optimal transmit beamforming at the BS is given by [14]

$$w_m^{\text{opt}} = \sqrt{\frac{P_t}{M}} e^{j\frac{2\pi}{\lambda}\bar{g}_m}, \forall m \in \mathcal{M}. \quad (19)$$

It is observed from (19) that the optimal transmit beamforming at the BS is independent of the user location \mathbf{p}_U . Given $\{w_m^{\text{opt}}\}$ and Ω , we configure the reflection coefficient matrix of the IRS as

$$\psi_n^{\text{opt}} = \text{mod} \left(\frac{2\pi}{\lambda} (\bar{g}_n + r_n), 2\pi \right), \forall n \in \mathcal{N}. \quad (20)$$

With $w_m^{\text{opt}}, \forall m = 1, \dots, M$ and $\psi_n^{\text{opt}}, \forall n = 1, \dots, N$, the received power is given by $P_r = \frac{4\pi\bar{l}^4\beta^2 P_t}{\lambda^2 M} \left| \sum_{n=1}^N \frac{\alpha_n \gamma_n}{r_n} \sum_{m=1}^M \frac{1}{t_{n,m}} \right|^2$. To facilitate the calculation of channel amplitudes, we consider the far-field case and approximate $t_{n,m} \approx t$, $r_n \approx r$, $\theta_n^i \approx \theta^i$, $\theta_n^r \approx \theta^r$, $\phi_n^i \approx \phi^i$, $\phi_n^r \approx \phi^r$, where θ_n^i , θ_n^r , ϕ_n^i , and ϕ_n^r are the azimuth and elevation angles of the incident angle and the reflected wave of the center of the IRS. Then, it follows that $\alpha_n \approx \alpha$, $\gamma_n \approx \gamma$, $q_n \approx q$. As such, the received power is expressed as

$$P_r = \frac{4\pi\bar{l}^4\beta^2 P_t M N^2 \alpha^2 \gamma^2}{\lambda^2 t^2 r^2}. \quad (21)$$

It is observed from (21) that the received power is in the order of $\mathcal{O}(\bar{l}^4)$, increases linearly with the number of the BS antenna and transmit power, and quadratically with the number of the IRS elements. Moreover, the received power is dependent on the reception and reflection factors of the IRS, which are determined by the incident and reflection angles. In the following, we characterize the relationship between the incident/reflection angles and the IRS rotation angles to highlight the important role of the rotation angles design in the system performance.

The three unit vectors of the local CCS at the IRS are expressed in the global CCS as

$$\mathbf{e}_x = (\cos\theta \sin\varphi, -\sin\theta \sin\varphi, -\cos\varphi)^T, \quad (22)$$

$$\mathbf{e}_y = (\sin\theta, \cos\theta, 0)^T, \quad (23)$$

$$\mathbf{e}_z = (\cos\theta \cos\varphi, -\sin\theta \cos\varphi, \sin\varphi)^T. \quad (24)$$

Then, the orientation matrix that characterizes the relationship from the global CCS to the local CCS at the IRS is given by

$$\mathbf{Q}(\theta, \varphi) = (\mathbf{e}_x, \mathbf{e}_y, \mathbf{e}_z) = \begin{bmatrix} \cos\theta \sin\varphi & \sin\theta & \cos\theta \cos\varphi \\ -\sin\theta \sin\varphi & \cos\theta & -\sin\theta \cos\varphi \\ -\cos\varphi & 0 & \sin\varphi \end{bmatrix}. \quad (25)$$

In the initial stage, the unit vectors along the x -, y -, z -axis of the local CCS are given by $\mathbf{e}_x = (0, 0, -1)^T$, $\mathbf{e}_y = (0, 1, 0)^T$,

$\mathbf{e}_z = (1, 0, 0)^T$, respectively, which are aligned with the negative z -, y -, and x -axis unit vectors of the global CCS. Based on (25), the coordinates in the IRS local CCS that correspond to any 3D location \mathbf{p} in the global CCS can be expressed as

$$\mathbf{p}^L = \mathbf{Q}^T(\theta, \varphi)(\mathbf{p} - \mathbf{p}_c) = (x^L, y^L, z^L)^T, \quad (26)$$

where we set \mathbf{p}_c as the IRS reference element at the origin of the corresponding local CCS. The coordinates of the BS and the user in the local CCS at the IRS are given by

$$\mathbf{p}_B^L = \mathbf{Q}^T(\theta, \varphi)(\mathbf{p}_B - \mathbf{p}_c) = [x_B^L, y_B^L, z_B^L]^T, \quad (27)$$

$$\mathbf{p}_U^L = \mathbf{Q}^T(\theta, \varphi)(\mathbf{p}_U - \mathbf{p}_c) = [x_U^L, y_U^L, z_U^L]^T. \quad (28)$$

Therefore, the azimuth angle of the incident wave of the center of the IRS $\theta^i \in [0, 2\pi]$, the azimuth angle of the reflected wave of the center of the IRS $\theta^r \in [0, 2\pi]$, the elevation angle of the incident wave of the center of the IRS $\phi^i \in [0, \pi/2]$, and the elevation angle of the reflected wave of the center of the IRS $\phi^r \in [0, \pi/2]$ are rewritten as

$$\theta^i = \arctan \frac{-y_B^L}{x_B^L}, \quad (29)$$

$$\theta^r = \arctan \frac{y_U^L}{x_U^L}, \quad (30)$$

$$\phi^i = \arccos \frac{z_B^L}{\|\mathbf{p}_B - \mathbf{p}_c\|}, \quad (31)$$

$$\phi^r = \arccos \frac{z_U^L}{\|\mathbf{p}_U - \mathbf{p}_c\|}. \quad (32)$$

Based on (27) and (28), (29), we can express (30), (31), and (32) with respect to θ and ϕ as

$$\theta^i = \arctan \frac{-x_B \sin \theta - (y_B - y_c) \cos \theta}{x_B \cos \theta \sin \varphi - (y_B - y_c) \sin \theta \sin \varphi + z_c \cos \varphi}, \quad (33)$$

$$\theta^r = \arctan \frac{x_U \sin \theta + (y_U - y_c) \cos \theta}{x_U \cos \theta \sin \varphi - (y_U - y_c) \sin \theta \sin \varphi + z_c \cos \varphi}, \quad (34)$$

$$\phi^i = \arccos \frac{x_B \cos \theta \cos \varphi - (y_B - y_c) \sin \theta \cos \varphi - z_c \sin \varphi}{\sqrt{x_B^2 + (y_B - y_c)^2 + z_c^2}}, \quad (35)$$

$$\phi^r = \arccos \frac{x_U \cos \theta \cos \varphi - \sin \theta \cos \varphi (y_U - y_c) - z_c \sin \varphi}{\sqrt{x_U^2 + (y_U - y_c)^2 + z_c^2}}. \quad (36)$$

We denote the normalized incident vector from the BS to the IRS and the normalized reflection vector from the IRS to the user as \mathbf{a}_t and \mathbf{a}_r , respectively, which are given by

$$\mathbf{a}_t = \frac{\mathbf{p}_c - \mathbf{p}_B}{\|\mathbf{p}_c - \mathbf{p}_B\|}, \quad (37)$$

$$\mathbf{a}_r = \frac{\mathbf{p}_U - \mathbf{p}_c}{\|\mathbf{p}_U - \mathbf{p}_c\|}. \quad (38)$$

To enable effective reflection, the BS and the user must be located in front of the IRS, which yields

$$\mathbf{a}_t^T \mathbf{k} \geq 0, \quad \mathbf{a}_r^T \mathbf{k} \leq 0. \quad (39)$$

Based on (26), we have $z_B^L \geq 0$ and $z_U^L \geq 0$. Then, it follows that

$$\begin{aligned} (x_B \cos \theta \cos \varphi - (y_B - y_c) \sin \theta \cos \varphi - z_c \sin \varphi) &\geq 0, \\ (x_U \cos \theta \cos \varphi - (y_U - y_c) \sin \theta \cos \varphi - z_c \sin \varphi) &\geq 0. \end{aligned} \quad (40)$$

Given $\{w_m^{\text{opt}}\}$ and $\{\phi_n^{\text{opt}}\}$, our objective is to maximize the minimum SNR over all locations within the target area \mathcal{A} by optimizing the rotation angles of the IRS. Therefore, the optimization problem can be formulated as

$$\max_{\Omega \in \mathcal{S}} \min_{\mathbf{p}_U \in \mathcal{A}} \varsigma \quad \text{s.t. (40)}. \quad (41)$$

Problem (41) is intractable for two main reasons. First, the objective function is defined as the minimum received power over a continuous region, which yields a semi-infinite and non-smooth formulation and generally lacks a closed-form expression of the IRS rotation angles. Second, problem (41) is non-convex, since the objective function is non-concave and the constraints are non-convex.

III. SINGLE TARGET LOCATION SNR MAXIMIZATION

In this section, we consider the special case of single target location power enhancement, where the target area \mathcal{A} reduces to the point \mathbf{p}_s . In this case, the inner minimization within problem (41) can be omitted. Thus, problem (41) can be reformulated as

$$\max_{\Omega \in \mathcal{S}} \varsigma \quad \text{s.t. (40)}. \quad (42)$$

Let $\bar{L} = \bar{l}/\lambda$ denote the wavelength-normalized length of each IRS element. With (21), problem (42) is reduced to

$$\max_{\Omega \in \mathcal{S}} \delta_1 \delta_2 \quad \text{s.t. (40)}, \quad (43)$$

where $\delta_1 = \cos^2 \phi^i (\cos^2 \phi^r \cos^2 (\theta^i + \theta^r) + \sin^2 (\theta^i + \theta^r))$ and $\delta_2 = \text{sinc}^2(\pi \bar{L} (\cos \theta^i \sin \phi^i + \sin \theta^r \cos \phi^r)) \times \text{sinc}^2(\pi \bar{L} (\sin \theta^r \sin \phi^r - \sin \theta^i \sin \phi^i))$.

The objective function of problem (43) consists of two terms δ_1 and δ_2 , where δ_2 composed of the $\text{sinc}(\cdot)$ function with the wavelength-normalized length \bar{L} . Without loss of generality, the IRS consists of a large number of passive reflecting elements with sub-wavelength inter-element spacing, i.e., $l = 0.5\lambda > \bar{l}$. Then, we have $\bar{L} < 0.5$. Motivated by the presence of the term δ_2 and the fact that $\text{sinc}(\cdot) \approx 1$ for small arguments, we characterize the impact of \bar{L} on the objective function. Figs. 4 and 5 illustrate the values of δ_1 , δ_2 , and $\delta_1 \delta_2$ versus the rotation angles Ω when $\bar{L} = 0.25$ and $\bar{L} = 0.1$, respectively. The BS, IRS, and user are located at $\mathbf{p}_B = [50, 20, 0]^T$, $\mathbf{p}_c = [0, 50, 10]^T$, and $\mathbf{p}_s = [30, 80, 0]^T$, respectively. It is observed from Figs. (4) and (5) that δ_2 exhibits less significant variations as the rotation angles change, as compared to δ_1 . This motivates us to focus on the rotation angles Ω that are designed to maximize δ_1 in the following. Problem (43) can be approximated as

$$\max_{\Omega \in \mathcal{S}} \cos^2 \phi^i (\cos^2 \phi^r \cos^2 (\theta^i + \theta^r) + \sin^2 (\theta^i + \theta^r)) \quad (44a)$$

$$\text{s.t. (40)}. \quad (44b)$$

Problem (44) is challenging to solve directly, since the objective function involves the complicated expression of the incident and reflection angles, which are functions of the optimization variables $\Omega = (\theta, \phi)^T$. We propose a tractable approach that yields a near-optimal solution, as expressed in the following proposition.

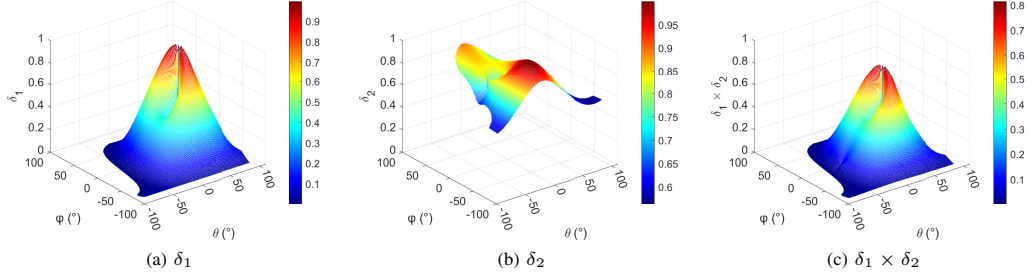


Fig. 4. Values of δ_1 , δ_2 , and $\delta_1 \times \delta_2$ versus the rotation Ω when $\bar{L} = 0.25$.

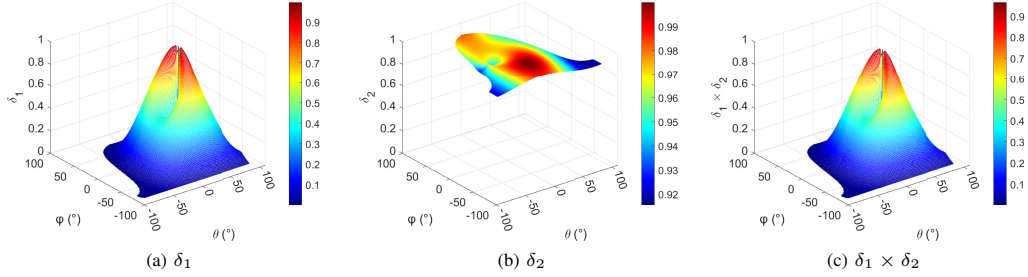


Fig. 5. Values of δ_1 , δ_2 , and $\delta_1 \times \delta_2$ versus the rotation Ω when $\bar{L} = 0.1$.

Proposition 3: Under the assumption that $\frac{(x_B(y_U - y_c) - x_U(y_B - y_c))\sqrt{x_B^2 + (y_B - y_c)^2 + z_c^2}}{z_c(x_B^2 + (y_B - y_c)^2 - x_B x_U - (y_U - y_c)(y_B - y_c))} \gg 1$, the optimized azimuth angle and elevation angle of the IRS can be given by $\theta^{\text{opt}} = \arctan\left(-\frac{y_B - y_c}{x_B}\right)$ and $\varphi^{\text{opt}} = \arctan\left(\frac{-z_c}{\sqrt{x_B^2 + (y_B - y_c)^2}}\right)$.

Proof: Please refer to Appendix C. ■

It is observed from Proposition 3 that the assumption is readily satisfied, especially when z_c approaches 0. In this case, the design of θ determines the system performance without the need for elevation rotation, i.e., $\varphi^{\text{opt}} = 0$. Moreover, the optimized elevation angle decreases as z_c increases while the azimuth angle remains unchanged. If the altitude of the IRS is sufficiently large, i.e., $z_c \rightarrow \infty$, we have $\phi^i = \phi^r \rightarrow \arccos(-\sin \varphi)$. The optimized azimuth angle of the IRS is approximated as $\varphi^{\text{opt}} = -\pi/2$ regardless of the value of θ while ensuring that constraint (40) holds. This is expected because both BS and the user are distributed on the ground, which is far from the IRS. The IRS acts as a point source, and beamforming gains depend primarily on optimizing ϕ rather than θ . If both BS and user are located far along the x -axis from the IRS, i.e., $x_B \rightarrow \infty$ and $x_U \rightarrow \infty$, it follows that $\phi^i = \phi^r \rightarrow \arccos(\cos \theta \cos \varphi)$. The optimal azimuth and elevation angles of the IRS are approximated as $\theta^{\text{opt}} = \varphi^{\text{opt}} = 0$. This implies that no rotation is needed, for similar reasons as in the case of $z_c \rightarrow \infty$.

By exploiting the specific structures of problem (43) and guided by the insights in Proposition 3, we propose an efficient PSO-based method, due to the following main issues: First, the particle swarm evaluates multiple candidates in parallel and cooperatively concentrates in the neighborhood of the near-optimal solution. Second, given the rotation constraints that ensures effective reflection, physical feasibility can be

incorporated into PSO by masking or projecting particles, thus avoiding wasted evaluations in infeasible sectors. Third, in the continuous angle domain rather than via grid search, PSO preserves global exploration and supports local refinement, which yields both robust global solutions and high-precision angular resolution. The processes of the proposed algorithm are provided as follows. The swarm is initialized with a high proportion of particles sampled in a small neighborhood around the high-quality solution, with the remaining particles sampled uniformly over the feasible domain. Thus, high-probability regions are reliably identified, and faster convergence is achieved than conventional PSO with random initialization. To ensure the effective reflection, i.e., constraint (40), each particle's performance is determined by a fitness function with an introduced penalty term as

$$\mathcal{L}(\Omega) = \delta_1 \delta_2 - \tau(\max\{0, -z_B^L\} + \max\{0, -z_U^L\}), \quad (45)$$

where τ is a penalty parameter satisfying $\tau > 0$. Let $\Omega_b^{(t)}$ and $\nu_b^{(t)}$ denote the position and velocity of the b -th particle at the t -th iteration. In each iteration, the position of each particle is updated as

$$\Omega_b^{(t+1)} = \mathcal{G}\left(\Omega_b^{(t)} + \nu_b^{(t)}\right), \quad (46)$$

where $\mathcal{G}(\cdot)$ is an element-wise projection operator that ensures $\Omega_b^{(t+1)} \in \mathcal{S}$. Let $\Omega_{b,\text{lbest}}$ and Ω_{gbest} denote the local best position of the b -th particle and the global best position among all particles, respectively. In the $(t+1)$ -th iteration, the velocity of the b -th particle can be expressed as

$$\begin{aligned} \nu_b^{(t+1)} &= \omega^{(t)} \nu_b^{(t)} + c_1 \cdot \text{rand} \cdot (\Omega_{b,\text{lbest}} - \Omega_b^{(t)}) \\ &\quad + c_2 \cdot \text{rand} \cdot (\Omega_{\text{gbest}} - \Omega_b^{(t)}), \end{aligned} \quad (47)$$

Algorithm 1: PSO-based Algorithm for Solving Problem (43)

Input: Number of particles B , maximum number of iterations T_{\max} , the cognitive coefficients c_1 , the social coefficients c_2 , the initial inertia weight ω_{ini} , the final inertia weight ω_{end} , \mathbf{p}_B , \mathbf{p}_c , \mathbf{p}_U , and \bar{L} .

Output: Ω^{opt} .

```

1 Initialize particle positions  $\{\Omega_1^{(0)}, \dots, \Omega_B^{(0)}\}$ , and velocities
   $\{\nu_1^{(0)}, \dots, \nu_B^{(0)}\}$ , local best positions  $\Omega_{b,\text{lbest}}$ , and global
  best position  $\Omega_{\text{gbest}}$ .
2 for  $t = 1$  to  $T_{\max}$  do
3   for  $b = 1$  to  $B$  do
4     Update  $\Omega_b^{(t)}$  via (46) and  $\nu_b^{(t)}$  via (47).
5     if  $\mathcal{L}(\Omega_b^{(t)}) > \mathcal{L}(\Omega_{b,\text{lbest}})$  then
6        $\Omega_{b,\text{lbest}} \leftarrow \Omega_b^{(t)}$ 
7     end
8     if  $\mathcal{L}(\Omega_{b,\text{lbest}}) > \mathcal{L}(\Omega_{\text{gbest}})$  then
9        $\Omega_{\text{gbest}} \leftarrow \Omega_{b,\text{lbest}}$ 
10    end
11  end
12 end
13 Return  $\Omega^{\text{opt}} = \Omega_{\text{gbest}}$ .
```

where c_1 and c_2 denote the cognitive and social coefficients, respectively. To balance the accuracy and convergence speed of the PSO, the inertia weight is denoted by

$$\omega^{(t)} = (\omega_{\text{ini}} - \omega_{\text{end}})(T_{\max} - t)/T_{\max} + \omega_{\text{end}}, \quad (48)$$

where T_{\max} is the number of iterations, ω_{ini} is the initial inertia weight, and ω_{end} is the final inertia weight. Based on both its own and the global best position, each particle iteratively updates its personal best position. Finally, the global best position is then updated by selecting the particle with the highest fitness value, ensuring a non-decreasing fitness value throughout the optimization process until convergence. The main procedures of the proposed PSO-based algorithm are summarized in Algorithm 1 with the computational complexity of $\mathcal{O}(2BT_{\max})$.

IV. AREA COVERAGE ENHANCEMENT

In this section, we consider the rotatable IRS-aided area coverage enhancement. Based on (21), problem (41) can be reduced to

$$\max_{\Omega \in \mathcal{S}} \min_{\mathbf{p}_U \in \mathcal{A}} \frac{\delta_1 \delta_2}{\|\mathbf{p}_U - \mathbf{p}_c\|^2} \quad \text{s.t. (40)}. \quad (49)$$

Problem (49) is still challenging to solve optimally via the conventional optimization methods. To solve this problem, we propose a PSO-based two-loop iterative algorithm in the following.

In the inner loop of our proposed algorithm, we calculate the value of the fitness function for each particle, which is given by

$$\mathcal{D}(\Omega) = \frac{\delta_1 \delta_2}{\|\mathbf{p}_U - \mathbf{p}_c\|^2} - \tau(\max\{0, -z_B^L\} + \max\{0, -z_U^L\}). \quad (50)$$

Thus, it follows that

$$\min_{\mathbf{p}_U \in \mathcal{A}} \mathcal{D}(\Omega_b^{(t)}), 1 \leq b \leq B, 1 \leq t \leq T_{\max}. \quad (51)$$

By exploiting the specific structure of problem (51), we first obtain the null points of δ_2 . For any rotation Ω , let Δ_1^{\max} and Δ_2^{\max} denote the maximum projection values, as well as Δ_1^{\min} and Δ_2^{\min} denote the minimum projection values within the target area \mathcal{A} , which are given by

$$\Delta_1^{\max} = \max_{\mathbf{p}_U \in \mathcal{A}} \cos \theta^i \sin \phi^i + \sin \theta^r \cos \phi^r, \quad (52)$$

$$\Delta_2^{\max} = \max_{\mathbf{p}_U \in \mathcal{A}} \sin \theta^r \sin \phi^r - \sin \theta^i \sin \phi^i, \quad (53)$$

$$\Delta_1^{\min} = \min_{\mathbf{p}_U \in \mathcal{A}} \cos \theta^i \sin \phi^i + \sin \theta^r \cos \phi^r, \quad (54)$$

$$\Delta_2^{\min} = \min_{\mathbf{p}_U \in \mathcal{A}} \sin \theta^r \sin \phi^r - \sin \theta^i \sin \phi^i. \quad (55)$$

The null points of δ_2 can be derived by setting $\pi \bar{L} \Delta_1 = \pm v_1 \pi$, $v_1 \in \mathcal{N}_+$, i.e., $\Delta_1 = \pm v_1 / \bar{L}$, or $\pi \bar{L} \Delta_2 = \pm v_2 \pi$, $v_2 \in \mathcal{N}_+$, i.e., $\Delta_2 = \pm v_2 / \bar{L}$. For any rotation Ω , the minimum value of δ_2 within \mathcal{A} is zero if there exist null points. It implies that the minimum value of $\delta_1 \delta_2$ within \mathcal{A} is zero. By prioritizing the detection of null points within the target region, i.e., $\delta_2 = 0$, it avoids exhaustive grid search over all user positions, thereby significantly reducing the computational complexity.

In the outer loop of our proposed algorithm, Algorithm 1 can be applied to optimize the reflection angle, which is designed to iteratively update the particle positions based on their individual and collective experiences. For each particle, the corresponding fitness value is evaluated in the inner loop.

The main procedures for solving problem 49 are summarized in Algorithm (2). The complexity of the inner-loop is $\mathcal{O}(A_x A_y)$ if no null point is detected. In the outer-loop, the complexity of the PSO-based method is $\mathcal{O}(2BT_{\max})$. Therefore, the overall complexity of our proposed algorithm is $\mathcal{O}(2BT_{\max} A_x A_y)$ in the worst case without null points.

V. SIMULATION RESULTS

In this section, simulation results are provided to evaluate the performance of our proposed design. The center of the BS, IRS, and target area, as well as the single target point are located at $\mathbf{p}_B = [50, 20, 0]^T$ m, $\mathbf{p}_c = [0, 50, 10]^T$ m, $\mathbf{p}_r = [30, 80, 0]^T$ m, and $\mathbf{p}_s = [30, 80, 0]^T$ m, respectively. The reference channel power gain is $\beta = -40$ dB. Other system parameters are set as: $M = 128$, $N = 256$, $\bar{L} = 0.25$, $A_x = A_y = 10$ m, $P_t = 30$ dBm, and $\sigma_0^2 = -90$ dBm. In the PSO-based algorithm, we set $B = 100$, $T_{\max} = 30$, $c_1 = c_2 = 2$, $\omega_{\text{ini}} = 0.4$, $\omega_{\text{end}} = 0.9$, and $\nu_b^{(t)} \in [-5, 5]$. For comparison, the following schemes are considered: 1) Fixed φ : the IRS can adjust its azimuth angle, while its elevation angle is fixed at $\varphi = 10^\circ$; 2) Fixed θ : the IRS can adjust its elevation angle, while its azimuth angle is fixed at $\theta = 10^\circ$; 3) Fixed rotation: the rotation angles of the IRS is fixed at $\Omega = \{0^\circ, 0^\circ\}$; 4) M-IRS: the IRS can move along y -axis with fixed rotation angles $\Omega = \{0^\circ, 0^\circ\}$.

A. Single Target Location SNR Enhancement

1) *Evaluation of the Proposed Schemes:* In Fig. 6, we consider the following schemes: 1) ES: the rotation angles is optimized via the exhaustive search method; 2) Proposed Opt: the rotation angles is optimized via Algorithm 1; 3) Proposed Subopt: the rotation angles is obtained in Proposition 3.

Algorithm 2: PSO-based Two-Loop Iterative Algorithm

Input: Number of particles B , maximum number of iterations T_{\max} , the cognitive coefficients c_1 , the social coefficients c_2 , the initial inertia weight ω_{ini} , the final inertia weight ω_{end} , \mathbf{p}_B , \mathbf{p}_c , \mathbf{p}_U , A_x , A_y , and \bar{L} .

Output: Ω^{opt} .

```

1 Initialize particle positions  $\{\Omega_1^{(0)}, \dots, \Omega_B^{(0)}\}$ , and velocities
 $\{\nu_1^{(0)}, \dots, \nu_B^{(0)}\}$ , local best positions  $\Omega_{b,\text{lbest}}$ , and global
best position  $\Omega_{\text{gbest}}$ .
2 for  $t = 1$  to  $T_{\max}$  do
3   for  $b = 1$  to  $B$  do
4     Update  $\Omega_b^{(t)}$  and  $\nu_b^{(t)}$ .
5     for  $x_U = x_r - A_x/2$  to  $x_r + A_x/2$  do
6       for  $y_U = y_r - A_y/2$  to  $y_r + A_y/2$  do
7         Calculate  $\theta^i$ ,  $\theta^r$ ,  $\phi^i$ , and  $\phi^r$  based on (33),
(34), (35), and (36).
8         Calculate  $\Delta_1$  and  $\Delta_2$ .
9         Update  $\Delta_1^{\min}$ ,  $\Delta_1^{\max}$ ,  $\Delta_2^{\min}$ , and  $\Delta_2^{\max}$ .
10        end
11      end
12      Obtain the minimum value of  $\delta_1\delta_2$  within  $\mathcal{A}$  as
 $\mathcal{L}(\Omega_b^{(t)})$ .
13      if  $\mathcal{D}(\Omega_b^{(t)}) > \mathcal{D}(\Omega_{b,\text{lbest}})$  then
14         $\Omega_{b,\text{lbest}} \leftarrow \Omega_b^{(t)}$ 
15      end
16      if  $\mathcal{D}(\Omega_{b,\text{lbest}}) > \mathcal{D}(\Omega_{\text{gbest}})$  then
17         $\Omega_{\text{gbest}} \leftarrow \Omega_{b,\text{lbest}}$ 
18      end
19    end
20  end
21 Return  $\Omega^{\text{opt}} = \Omega_{\text{gbest}}$ .

```

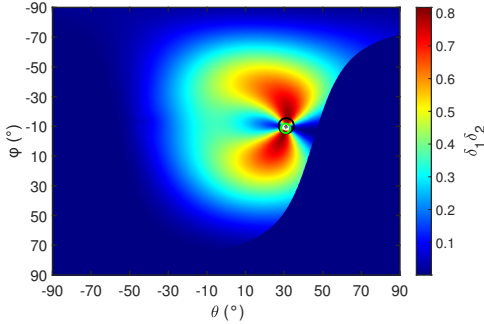


Fig. 6. $\delta_1\delta_2$ versus the azimuth angle θ and elevation angle φ , where the optimized rotation angles $\Omega^{\text{opt}} = \{\theta^{\text{opt}}, \varphi^{\text{opt}}\}$ obtained by the exhaustive search method, Algorithm 1, and the closed form in Proposition 3 are marked with black, green, and white circles, respectively.

Fig. 6 shows the value of $\delta_1\delta_2$ versus the azimuth angle θ and elevation angle φ . One can observe that there exists truncation with a substantial region where the value of $\delta_1\delta_2$ approaches zero, indicating that the corresponding rotation angles fail to satisfy the constraints under the considered system setup. This highlights the importance of rotation optimization, as a considerable performance gain can be obtained by properly adjusting θ and φ . Furthermore, it is observed that all three schemes yield nearly identical optimal rotation angles Ω . Moreover, the elevation angle φ is negative, which is expected since both the BS and the user are located below the IRS. The

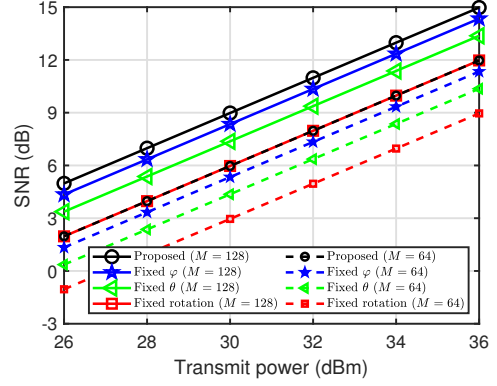


Fig. 7. SNR versus transmit power.

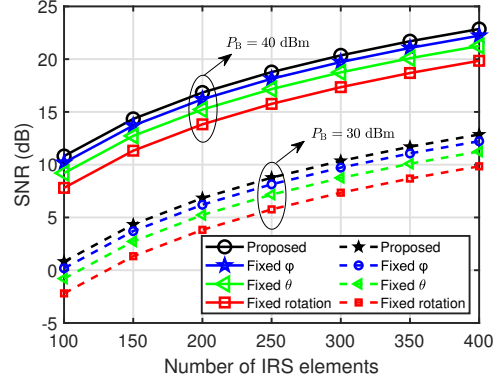


Fig. 8. SNR versus the number of the IRS elements.

results demonstrate the effectiveness of the solution obtained by Algorithm 1 and the closed form in achieving performance comparable to that by the exhaustive search method but with lower computational complexity.

2) *Performance Comparison for Rotatable IRS and Fixed Rotation IRS:* In Fig. 7, we plot the SNR versus the maximum transmit power at the BS for both $M = 128$ and $M = 64$. First, one can observe that the SNR of all the schemes monotonically increases with P_t and M due to the higher beamforming gain provided by the BS. Second, it is observed that the proposed scheme outperforms other schemes, and the performance gap between the fixed rotation scheme and the proposed scheme is 3 dB. Moreover, we observe that the proposed scheme, even when deploying half the number of antennas at the BS, i.e., $M = 64$, is able to achieve almost the same performance as the fixed rotation scheme with $M = 128$. Based on (21), which states that the received signal power is linearly proportional to the number of antennas, halving the antenna number introduces a 3 dB performance loss. The fact that the proposed scheme with $M = 64$ can compensate for this theoretical loss and match the performance of the benchmark with $M = 128$ demonstrates the effectiveness of the proposed scheme and highlights the importance of the IRS rotation.

In Fig. 8, we plot the SNR versus the number of the IRS elements for both $P_t = 30$ dBm and $P_t = 40$ dBm. It is observed that the SNR of all the schemes monotonically increases with

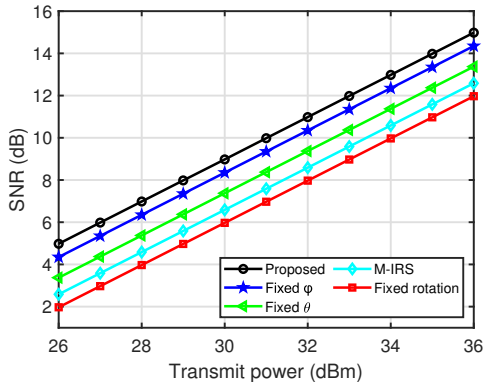


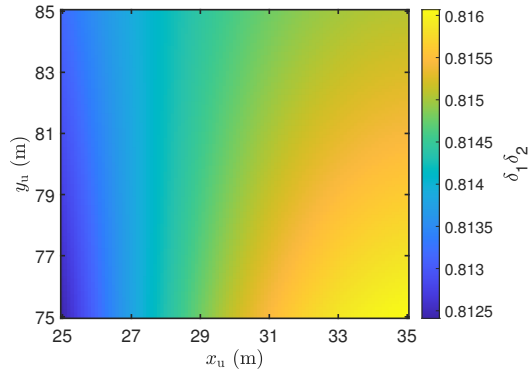
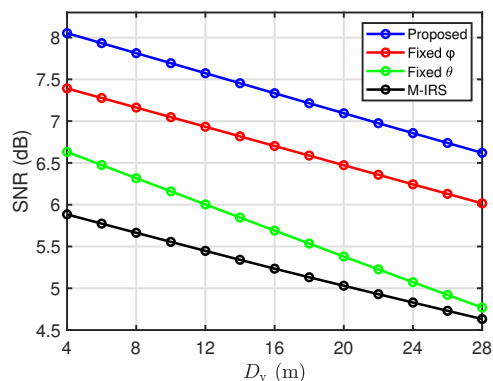
Fig. 9. SNR versus transmit power.

N , which can be attributed to the fact that a larger number of reflecting elements contributes to higher passive beamforming gains, thereby enhancing the power of the received signal. Note that to achieve an SNR of 20 dB, the required number of IRS elements is reduced from 400 to 300 by replacing the fixed rotation scheme with the proposed scheme, which indicates that the proposed scheme substantially reduces the hardware requirements for the IRS configuration. The reason is that the proposed scheme provides larger effective reception and reflection factors that can effectively compensate for the performance degradation caused by the reduction in the number of the IRS elements.

3) *Performance Comparison for Rotatable IRS and M-IRS:* Fig. 9 shows the SNR versus the transmit power. Compared to the fixed rotation scheme, where the IRS is unrotatable and unmovable, the M-IRS yields a higher SNR by additionally adjusting its placement. It is observed that the three schemes with rotatable IRS, even when only optimizing the azimuth angle or the elevation angle, perform better than that with M-IRS under different transmit power, thanks to the flexible rotation angles adjustment. Moreover, the SNR of the proposed scheme significantly outperforms other benchmark schemes. The result is expected since the proposed scheme can fully exploit the spatial design DoF of rotation, which highlights the potential of dynamically adjusting IRS rotation for single target location SNR enhancement.

B. Area Coverage Enhancement

1) *Performance Evaluation Under Locations within the Target Area:* Fig. 10 shows the SNR at different locations within \mathcal{A} for IRS-aided area coverage enhancement with the proposed scheme. It is observed that at any location within the target coverage area, an approximately equal value of $\delta_1\delta_2$ can be achieved, with all values being larger than 0.8124. Since $\delta_1\delta_2$ is a function of the reception and reflection factors of the IRS, the spatial uniformity across the target area indicates that the IRS not only efficiently captures the incident energy from the BS but also efficiently reflects it toward the user, irrespective of its specific locations. By optimizing the IRS rotation angles Ω , the system enables intelligent signal energy focusing and spatial distribution, which fully exploits the potential of the IRS in terms of SNR enhancement. The results

Fig. 10. SNR at different locations within \mathcal{A} .Fig. 11. SNR versus the length of the target area, D_y .

strongly validate the effectiveness of the proposed scheme in enhancing the performance of the target coverage area.

In Fig. 11, we plot the worst-case SNR versus the length of the target area, D_y . It is observed that all the schemes monotonically decrease as D_y increases, with the fixed θ scheme exhibiting a more pronounced decline. For example, when D_y increases from 4 m to 28 m, the SNR achieved by the fixed θ scheme drops from 6.6 dB to 4.7 dB, while the other three schemes experience a decrease of less than 1.5 dB. This is because the horizontal distance from the IRS to the edge of the target area becomes more significant, making the optimization of θ increasingly critical for target coverage enhancement. Nevertheless, the fixed θ scheme outperforms the M-IRS scheme across the entire range of D_y in terms of SNR, particularly when the area length is relatively small. As the area size increases, it becomes increasingly challenging to achieve effective area coverage by optimizing only azimuth angle or elevation angle, due to the effective reflection constraints. Compared to the benchmark schemes, the proposed scheme achieves the best performance, which yields a significant performance gain over the other schemes. The results indicate that the IRS with the optimized rotation angles can fully exploit the spatial DoFs offered by the rotation design.

2) *Impact of the IRS's Altitude:* In Fig. 12(a), we plot the worst-case SNR versus the IRS's altitude z_c . One can observe that the schemes with optimized φ , i.e., the proposed scheme

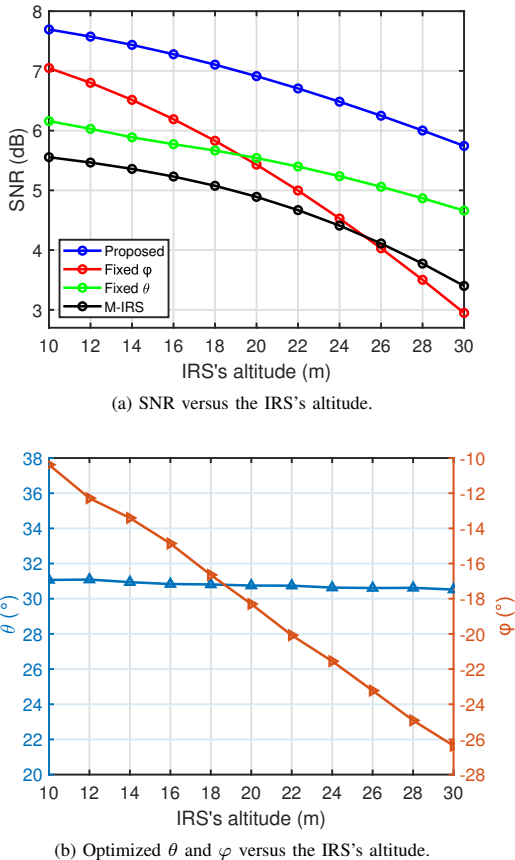


Fig. 12. Comparison on SNR and the optimized IRS rotation versus the IRS's altitude.

and the fixed θ scheme, outperform the M-IRS scheme under different z_c . Moreover, we observe that the SNR of all the schemes monotonically decreases as z_c increases due to the increased path loss, with the fixed φ scheme showing the sharpest decline. For example, as z_c increases from 18 m to 30 m, the SNR achieved by the fixed φ scheme decreases from 5.8 dB to 2.9 dB. The gap between the schemes with and without optimized φ becomes more pronounced as z_c increases. This is because the vertical distance from the IRS to both the BS and the user becomes more significant, and optimizing the elevation angle φ becomes increasingly critical for SNR maximization. Nevertheless, the fixed φ scheme performs better than the M-IRS scheme in a wide range of the IRS's altitude. In Fig. 12(b), we plot the azimuth and elevation angle of the IRS optimized by Algorithm 2 versus the IRS's altitude. It is observed that the absolute value of the elevation angle increases significantly with z_c . In contrast, the optimized azimuth angle remains almost unchanged. It is because as the IRS's altitude increases, more vertical steering is required to aim at the x - y plane, where the BS and user are located. The results demonstrate that optimizing φ has a greater impact on improving the SNR than optimizing θ , which are the same as Fig. 12(a).

VI. CONCLUSION

This paper has studied the rotatable IRS-aided wireless communication system under a practical angle-dependent channel

model. Based on the developed model, the closed-form SNR expression was derived to unveil the effects of IRS geometry, rotation, and electromagnetic factors modeling. PSO-based algorithms were developed to efficiently solve the optimization problem for SNR maximization. Numerical results demonstrated that the rotatable IRS outperformed the M-IRS baseline in extending the coverage range with fewer BS antennas, transmit power, and reflecting elements. For the single target location case, it was shown that the proposed scheme achieves an approximately 3 dB SNR gain over the conventional fixed IRS scheme. For the area coverage case, adjusting the elevation angle of the IRS was shown to have a greater impact than tuning its azimuth angle on system performance at higher IRS altitudes. These findings provide useful guidelines for deploying the rotatable IRS in future wireless systems.

APPENDIX A: PROOF OF PROPOSITION 1

Based on (6) and (10), it follows that

$$t_{n,m} = \left\| \mathbf{p}_{B,1} + M_m^c \tilde{\mathbf{l}} \mathbf{m}_B^c + M_m^r \tilde{\mathbf{l}} \mathbf{m}_B^r - \mathbf{p}_1 - N_n^c \mathbf{l} \mathbf{m}_c - N_n^r \mathbf{l} \mathbf{m}_r \right\| \\ = \left\| \mathbf{d}_{1,1} + \Delta_{m,n} \right\|, n \in \mathcal{N}, m \in \mathcal{M}, \quad (56)$$

where $\mathbf{d}_{1,1} = \mathbf{p}_{B,1} - \mathbf{p}_1$ and $\Delta_{m,n} = M_m^c \tilde{\mathbf{l}} \mathbf{m}_B^c + M_m^r \tilde{\mathbf{l}} \mathbf{m}_B^r - N_n^c \mathbf{l} \mathbf{m}_c - N_n^r \mathbf{l} \mathbf{m}_r$ stands for the offset vector introduced by the array element indices. To facilitate the calculation, $\Delta_{m,n}$ is decomposed w.r.t. $\mathbf{d}_{1,1}$. Assuming that the distance between the 1-th BS antenna and 1-th element of the IRS is larger than the size of the IRS, the component of $\Delta_{m,n}$ parallel to $\mathbf{d}_{1,1}$ with magnitude $\bar{\Delta}$, contributes directly to the propagation distance, whereas its orthogonal component with magnitude $\tilde{\Delta}$, produces spatial deviation without affecting the distance magnitude. Then, it follows that

$$\bar{\Delta} = \frac{\Delta_{m,n} \cdot \mathbf{d}_{1,1}}{\|\Delta_{m,n}\| \cdot \|\mathbf{d}_{1,1}\|} = \frac{1}{t_{1,1}} \left(M_m^c \tilde{\mathbf{l}} \mathbf{m}_B^c \cdot \mathbf{d}_{1,1} + M_m^r \tilde{\mathbf{l}} \mathbf{m}_B^r \cdot \mathbf{d}_{1,1} - N_n^c \mathbf{l} \mathbf{m}_c \cdot \mathbf{d}_{1,1} - N_n^r \mathbf{l} \mathbf{m}_r \cdot \mathbf{d}_{1,1} \right), n \in \mathcal{N}, m \in \mathcal{M}. \quad (57)$$

With ϖ_B^c , ϖ_B^r , ϖ_c , and ϖ_r , we have

$$\bar{\Delta} = M_m^c \tilde{l} \cos \varpi_B^c + M_m^r \tilde{l} \cos \varpi_B^r - N_n^c l \cos \varpi_c - N_n^r l \cos \varpi_r, n \in \mathcal{N}, m \in \mathcal{M}. \quad (58)$$

According to the Pythagorean theorem, we have

$$t_{n,m} = \sqrt{(t_{1,1} + \bar{\Delta})^2 + \tilde{\Delta}^2}, n \in \mathcal{N}, m \in \mathcal{M}. \quad (59)$$

Note that $t_{n,m}$ is a function with respect to $\tilde{\Delta}$ and thus we use $t_{n,m}(\tilde{\Delta})$ to represent $t_{n,m}$. When expanded by a Taylor series at $\tilde{\Delta} = 0$, $t_{n,m}(\tilde{\Delta})$ can be represented as

$$t_{n,m}(\tilde{\Delta}) \approx t_{n,m}(0) + t'_{n,m}(0) \tilde{\Delta}. \quad (60)$$

Then, we can omit the second term since $\tilde{\Delta}$ is small, and approximate $t_{n,m}$ as

$$t_{n,m} \approx t_{1,1} + \bar{\Delta} \\ = t_{1,1} + M_m^c \tilde{l} \cos \varpi_B^c + M_m^r \tilde{l} \cos \varpi_B^r - N_n^c l \cos \varpi_c - N_n^r l \cos \varpi_r, n \in \mathcal{N}, m \in \mathcal{M}. \quad (61)$$

By substituting $t_{n,m}$ into (14), the proof is completed.

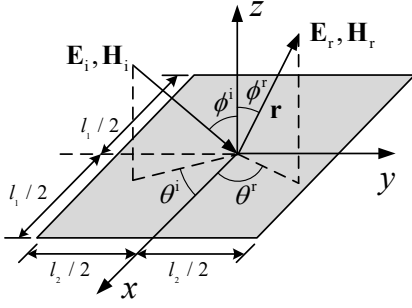


Fig. 13. An example of electromagnetic wave scattering by a metal plate.

APPENDIX B: PROOF OF PROPOSITION 2

We consider a perfectly conducting rectangular plate with dimensions $l_1 \times l_2$ and negligible thickness, located in the $x-y$ plane. A distant point source radiates linearly polarized waves with wave number $k = \frac{2\pi}{\lambda}$. As shown in Fig. 13, let θ^i , ϕ^i , θ^r , and ϕ^r denote the azimuth and elevation angles of the incident wave of the center of plane, as well as the elevation and azimuth angles of the reflected wave of the center of plane. The electric and magnetic field components of the incident wave is given by [44], [45]

$$\mathbf{E}_i = E_i (\mathbf{e}_x \sin \theta^i + \mathbf{e}_y \cos \theta^i) \times e^{-jk(-x \sin \phi^i \cos \theta^i + y \sin \phi^i \sin \theta^i - z \cos \phi^i)}, \quad (62)$$

$$\mathbf{H}_i = \frac{E_i}{\mu} (\mathbf{e}_x \cos \theta^i \cos \phi^i - \mathbf{e}_y \sin \theta^i \cos \phi^i - \mathbf{e}_z \sin \phi^i) \times e^{-jk(-x \sin \phi^i \cos \theta^i + y \sin \phi^i \sin \theta^i - z \cos \phi^i)}, \quad (63)$$

where μ is the characteristic impedance of the medium. Given the negligible thickness of the plane Q , the induced surface current density can be approximated

$$\begin{aligned} \mathbf{J}_Q &\approx 2\mathbf{e}_z \times \mathbf{H}_i|_{z=0, x=x', y=y'} \\ &= \frac{2E_i}{\mu} (\mathbf{e}_x \cos \theta^i \cos \phi^i - \mathbf{e}_y \sin \theta^i \cos \phi^i) \\ &\quad \times e^{-jk(-x' \sin \phi^i \cos \theta^i + y' \sin \phi^i \sin \theta^i)}. \end{aligned} \quad (64)$$

Then, we have

$$J_x = \frac{2E_i}{\mu} \cos \theta^i \cos \phi^i e^{-jk(-x' \sin \phi^i \cos \theta^i + y' \sin \phi^i \sin \theta^i)}, \quad (65)$$

$$J_y = -\frac{2E_i}{\mu} \sin \theta^i \cos \phi^i e^{-jk(-x' \sin \phi^i \cos \theta^i + y' \sin \phi^i \sin \theta^i)}, \quad (66)$$

$$J_z = 0. \quad (67)$$

Let $\mathbf{r}' = (x', y', 0)^T$ denotes the position vector on the plate and ζ represents the angle between \mathbf{r} and \mathbf{r}' . Then, we have $r' \cos \zeta = x' \sin \theta^r \cos \phi^r + y' \sin \theta^r \sin \phi^r$. By introducing an intermediate vector $\mathbf{T} = \int \int_Q \mathbf{J}_Q e^{jk r' \cos \zeta} dq'$, it follows that

$$T_x = \int \int J_x e^{jk r' \cos \zeta} dx' dy', \quad (68)$$

$$T_y = \int \int J_y e^{jk r' \cos \zeta} dx' dy', \quad (69)$$

$$T_z = 0, \quad (70)$$

when $z' = 0$. With the rectangular-to-spherical component transformation given by

$$\begin{bmatrix} T_r \\ T_\theta \\ T_\phi \end{bmatrix} = \begin{bmatrix} \cos \theta \sin \phi & \sin \theta \sin \phi & \cos \phi \\ \cos \theta \cos \phi & \sin \theta \cos \phi & -\sin \phi \\ -\sin \theta & \cos \theta & 0 \end{bmatrix} \begin{bmatrix} T_x \\ T_y \\ T_z \end{bmatrix}, \quad (71)$$

it follows that

$$T_\theta = \frac{2E_i l_1 l_2}{\mu} \cos \phi^i \cos \phi^r \cos(\theta^i + \theta^r) \text{sinc}(X) \text{sinc}(Y), \quad (72)$$

$$T_\phi = -\frac{2E_i l_1 l_2}{\mu} \cos \phi^i \sin(\theta^i + \theta^r) \text{sinc}(X) \text{sinc}(Y), \quad (73)$$

where $X = \frac{\pi l_1}{\lambda} (\cos \theta^i \sin \phi^i + \sin \theta^r \cos \phi^r)$ and $Y = \frac{\pi l_2}{\lambda} (\sin \theta^r \sin \phi^r - \sin \theta^i \sin \phi^i)$. Assuming that the plate is a perfect electric conductor and in the far-field case, the scattered electric field magnitude is approximated by $|E_r| = \sqrt{|E_\theta|^2 + |E_\phi|^2}$, where $E_\theta \approx -\frac{jke^{-jkr}}{4\pi r} \mu T_\theta$ and $E_\phi \approx -\frac{jke^{-jkr}}{4\pi r} \mu T_\phi$ with $r = |\mathbf{r}|$. As such, the ratio of the scattered electric field magnitude to the incident electric field magnitude is given by

$$\frac{|E_r|}{|E_i|} = \frac{l_1 l_2}{\lambda r} \cos \phi^i Z \text{sinc}(X) \text{sinc}(Y), \quad (74)$$

where $Z = \sqrt{\cos^2 \phi^r \cos^2(\theta^i + \theta^r) + \sin^2(\theta^i + \theta^r)}$. After removing the path loss factor, i.e., $1/r$, and applying the spherical normalization used in radar cross section (RCS), i.e., 4π , the reflection coefficient of the metal plate without the IRS phase shift is given by

$$\bar{\eta} = \sqrt{\frac{4\pi l_1^2 l_2^2}{\lambda^2}} \cos \phi^i Z \text{sinc}(X) \text{sinc}(Y). \quad (75)$$

Thus, the proof is completed.

APPENDIX C: PROOF OF PROPOSITION 3

Given that both squared terms are non-negative, assuming that the objective function of problem (44) can reach its maximum value of 1, i.e., $\delta_1 = 1$, then we have $\cos^2 \phi^i = 1$ and $\cos^2 \phi^r \cos^2(\theta^i + \theta^r) + \sin^2(\theta^i + \theta^r) = 1$. Two feasible solutions that satisfy the above conditions are given by

$$\begin{cases} \phi^i = 0, \\ \theta^i = 0, \\ \theta^r = \pi/2, \end{cases} \quad \text{and} \quad \begin{cases} \phi^i = 0, \\ \theta^i = 0, \\ \theta^r = 3\pi/2. \end{cases} \quad (76)$$

With both solutions, we have $\theta^i = 0$. Substituting $\phi^i = 0$ into (33) yields the following equation for the optimized azimuth angle: $x_B \sin \theta^{\text{opt}} + (y_B - y_c) \cos \theta^{\text{opt}} = 0$. Thus, we have $\theta^{\text{opt}} = \arctan\left(-\frac{y_B - y_c}{x_B}\right)$. Given $\phi^i = 0$, by substituting θ^{opt} into (35), the equation for the optimized elevation angle is given by $\sqrt{x_B^2 + (y_B - y_c)^2} \cos \varphi^{\text{opt}} - z_c \sin \varphi^{\text{opt}} = \sqrt{x_B^2 + (y_B - y_c)^2 + z_c^2}$. Thus, we have $\varphi^{\text{opt}} = \arctan\left(\frac{-z_c}{\sqrt{x_B^2 + (y_B - y_c)^2}}\right)$. By substituting θ^{opt} and φ^{opt} into (34), we have

$$\theta^r = \arctan\left(\frac{x_B(y_U - y_c) - x_U(y_B - y_c) \sqrt{x_B^2 + (y_B - y_c)^2 + z_c^2}}{z_c(x_B^2 + (y_B - y_c)^2 - x_B x_U - (y_U - y_c)(y_B - y_c))}\right). \quad (77)$$

Assuming that $\frac{(x_B(y_U - y_C) - x_U(y_B - y_C))\sqrt{x_B^2 + (y_B - y_C)^2 + z_C^2}}{z_C(x_B^2 + (y_B - y_C)^2 - x_B x_U - (y_U - y_C)(y_B - y_C))} \gg 1$, θ^r can be approximated as $\pi/2$, which completes the proof.

REFERENCES

- [1] Q. Wu *et al.*, "Intelligent surfaces empowered wireless network: Recent advances and the road to 6G," *Proc. IEEE*, vol. 112, no. 7, pp. 724–763, Jul. 2024.
- [2] Z. Kang, C. You, and R. Zhang, "Active-IRS-aided wireless communication: Fundamentals, designs and open issues," *IEEE Wireless Commun.*, vol. 31, no. 3, pp. 368–374, Jun. 2024.
- [3] Q. Xue *et al.*, "A survey of beam management for mmwave and THz communications towards 6G," *IEEE Commun. Surv. Tutorials*, vol. 26, no. 3, pp. 1520–1559, 3rd Quart. 2024.
- [4] X. Pang, W. Mei, N. Zhao, and R. Zhang, "Intelligent reflecting surface assisted interference mitigation for cellular-connected UAV," *IEEE Wireless Commun. Lett.*, vol. 11, no. 8, pp. 1708–1712, Aug. 2022.
- [5] Y. Song and S. Xu, "Robust beamforming for IRS-aided multi-cell mmwave communication systems," *IEEE Trans. Veh. Technol.*, vol. 72, no. 7, pp. 9189–9205, July. 2023.
- [6] G. Chen *et al.*, "Active IRS aided multiple access for energy-constrained IoT systems," *IEEE Trans. Wireless Commun.*, vol. 22, no. 3, pp. 1677–1694, Mar. 2023.
- [7] Q. Peng *et al.*, "Hybrid active-passive IRS assisted energy-efficient wireless communication," *IEEE Commun. Lett.*, vol. 27, no. 8, pp. 2202–2206, Aug. 2023.
- [8] Z. Kang, C. You, and R. Zhang, "Double-active-IRS aided wireless communication: Deployment optimization and capacity scaling," *IEEE Wireless Commun. Lett.*, vol. 12, no. 11, pp. 1821–1825, Nov. 2023.
- [9] J. Feng *et al.*, "Joint passive beamforming and deployment design for dual distributed-IRS aided communication," *IEEE Trans. Veh. Technol.*, vol. 72, no. 10, pp. 13 758–13 763, Oct. 2023.
- [10] M. Fu, L. Zhu, and R. Zhang, "Multi-IRS enhanced wireless coverage: Deployment optimization based on large-scale channel knowledge," *IEEE Trans. Wireless Commun.*, early access, 2025, doi: 10.1109/TWC.2025.3570475.
- [11] Y. Han, S. Zhang, L. Duan, and R. Zhang, "Cooperative double-IRS aided communication: Beamforming design and power scaling," *IEEE Wireless Commun. Lett.*, vol. 9, no. 8, pp. 1206–1210, Aug. 2020.
- [12] Q. Peng *et al.*, "Joint size and placement optimization for IRS-aided communications with active and passive elements," *IEEE Trans. Commun.*, vol. 73, no. 9, pp. 7210–7225, Sep. 2025.
- [13] Q. Wu *et al.*, "Intelligent reflecting surfaces for wireless networks: Deployment architectures, key solutions, and field trials," *IEEE Wireless Commun.*, early access, 2025, doi: 10.1109/MWC.001.250002.
- [14] H. Lu, Y. Zeng, S. Jin, and R. Zhang, "Aerial intelligent reflecting surface: Joint placement and passive beamforming design with 3D beam flattening," *IEEE Trans. Wireless Commun.*, vol. 20, no. 7, pp. 4128–4143, Jul. 2021.
- [15] C. Liu *et al.*, "UAV-enabled passive 6D movable antennas: Joint deployment and beamforming optimization," *arXiv preprint arXiv:2412.11150*, 2024.
- [16] H. Jiang *et al.*, "Large-scale RIS enabled air-ground channels: Near-field modeling and analysis," *IEEE Trans. Wireless Commun.*, vol. 24, no. 2, pp. 1074–1088, Feb. 2025.
- [17] P. Wang, W. Mei, J. Fang, and R. Zhang, "Target-mounted intelligent reflecting surface for joint location and orientation estimation," *IEEE J. Sel. Areas Commun.*, vol. 41, no. 12, pp. 3768–3782, Dec. 2023.
- [18] Z. Ning *et al.*, "6G communication new paradigm: The integration of unmanned aerial vehicles and intelligent reflecting surfaces," *IEEE Commun. Surveys Tuts.*, early access, 2025, doi: 10.1109/COMST.2025.3526251.
- [19] Y. Ge *et al.*, "Intelligent reflecting surface-enhanced UAV communications: Advances, challenges, and prospects," *IEEE Wireless Commun.*, vol. 30, no. 6, pp. 119–126, Dec. 2023.
- [20] D. Xu, Y. Sun, D. W. K. Ng, and R. Schober, "Multiuser MISO UAV communications in uncertain environments with no-fly zones: Robust trajectory and resource allocation design," *IEEE Trans. Commun.*, vol. 68, no. 5, pp. 3153–3172, May 2020.
- [21] J. Wang *et al.*, "Power control and passive beamforming for the STAR-RIS with rotatable angles," *IEEE Trans. Veh. Technol.*, vol. 73, no. 8, pp. 12 121–12 125, Aug. 2024.
- [22] G. Ghatak, "On the placement of intelligent surfaces for RSSI-based ranging in mm-wave networks," *IEEE Commun. Lett.*, vol. 25, no. 6, pp. 2043–2047, Jun. 2021.
- [23] B. Li, D. Yang, and L. Liu, "Rotatable RIS-assisted edge computing: Orientation, task offloading, and resource optimization," *IEEE Trans. Veh. Technol.*, vol. 74, no. 8, pp. 13 290–13 295, Aug. 2025.
- [24] J. Wang *et al.*, "Rotatable RIS assisted physical layer multicasting," *arXiv preprint arXiv:2507.20113*, 2025.
- [25] T. Ji, M. Hua, C. Li, Y. Huang, and L. Yang, "Robust max-min fairness transmission design for IRS-aided wireless network considering user location uncertainty," *IEEE Trans. Commun.*, vol. 71, no. 8, pp. 4678–4693, Aug. 2023.
- [26] H. Wang *et al.*, "Passive six-dimensional movable antenna (6DMA)-assisted multiuser communication," *IEEE Wireless Commun. Lett.*, vol. 14, no. 4, pp. 1014–1018, Apr. 2025.
- [27] X. Shao, Q. Jiang, and R. Zhang, "6D movable antenna based on user distribution: Modeling and optimization," *IEEE Trans. Wireless Commun.*, vol. 24, no. 1, pp. 355–370, Jan. 2025.
- [28] X. Shao *et al.*, "6D movable antenna enhanced wireless network via discrete position and rotation optimization," *IEEE J. Sel. Areas Commun.*, vol. 43, no. 3, pp. 674–687, Mar. 2025.
- [29] X. Shao and R. Zhang, "6DMA enhanced wireless network with flexible antenna position and rotation: Opportunities and challenges," *IEEE Commun. Mag.*, vol. 63, no. 4, pp. 121–128, Apr. 2025.
- [30] B. Zheng, Q. Wu, T. Ma, and R. Zhang, "Rotatable antenna enabled wireless communication: Modeling and optimization," *arXiv preprint arXiv:2501.02595*, 2025.
- [31] H. Lu *et al.*, "Wireless communication with flexible reflector: Joint placement and rotation optimization for coverage enhancement," *IEEE Trans. Wireless Commun.*, early access, 2025, doi: 10.1109/TWC.2025.3564956.
- [32] B. Ning *et al.*, "Movable antenna-enhanced wireless communications: General architectures and implementation methods," *IEEE Wireless Commun.*, vol. 32, no. 5, pp. 108–116, Oct. 2025.
- [33] Z. Cui, K. Guan, J. Zhang, and Z. Zhong, "SNR coverage probability analysis of RIS-aided communication systems," *IEEE Trans. Veh. Technol.*, vol. 70, no. 4, pp. 3914–3919, Apr. 2021.
- [34] X. Cheng *et al.*, "Joint optimization for RIS-assisted wireless communications: From physical and electromagnetic perspectives," *IEEE Trans. Commun.*, vol. 70, no. 1, pp. 606–620, Jan. 2022.
- [35] Ö. Özdogan, E. Björnson, and E. G. Larsson, "Intelligent reflecting surfaces: Physics, propagation, and pathloss modeling," *IEEE Wireless Commun. Lett.*, vol. 9, no. 5, pp. 581–585, May 2020.
- [36] F. H. Danufane, M. D. Renzo, J. de Rosny, and S. A. Tretyakov, "On the path-loss of reconfigurable intelligent surfaces: An approach based on Green's theorem applied to vector fields," *IEEE Trans. Commun.*, vol. 69, no. 8, pp. 5573–5592, Aug. 2021.
- [37] G. Stratidakis, S. Droulias, and A. Alexiou, "Optimal position and orientation study of reconfigurable intelligent surfaces in a mobile user environment," *IEEE Trans. Antennas Propag.*, vol. 70, no. 10, pp. 8863–8871, Oct. 2022.
- [38] M. Najafi, V. Jamali, R. Schober, and H. V. Poor, "Physics-based modeling and scalable optimization of large intelligent reflecting surfaces," *IEEE Trans. Commun.*, vol. 69, no. 4, pp. 2673–2691, Apr. 2021.
- [39] W. Tang *et al.*, "Path loss modeling and measurements for reconfigurable intelligent surfaces in the millimeter-wave frequency band," *IEEE Trans. Commun.*, vol. 70, no. 9, pp. 6259–6276, Sep. 2022.
- [40] J. Liu and H. Zhang, "Max-min area coverage in IRS assisted networks: Rotatable design and experimental verification," *IEEE Trans. Commun.*, early access, 2025, doi: 10.1109/TCOMM.2025.3571960.
- [41] S. Zeng, H. Zhang, B. Di, Z. Han, and L. Song, "Reconfigurable intelligent surface (RIS) assisted wireless coverage extension: RIS orientation and location optimization," *IEEE Commun. Lett.*, vol. 25, no. 1, pp. 269–273, Jan. 2021.
- [42] Y. Han, S. Zhang, L. Duan, and R. Zhang, "Double-IRS aided MIMO communication under LoS channels: Capacity maximization and scaling," *IEEE Trans. Commun.*, vol. 70, no. 4, pp. 2820–2837, Apr. 2022.
- [43] H. Jiang, B. Xiong, H. Zhang, and E. Basar, "Physics-based 3D end-to-end modeling for double-RIS assisted non-stationary UAV-to-ground communication channels," *IEEE Trans. Commun.*, vol. 71, no. 7, pp. 4247–4261, Jul. 2023.
- [44] H. Luo *et al.*, "A generalized model for RIS-assisted communications: On the effect of scattered electromagnetic wave," *IEEE Wirel. Commun. Lett.*, vol. 13, no. 4, pp. 1143–1147, Apr. 2024.
- [45] Ö. Özdogan, E. Björnson, and E. G. Larsson, "Intelligent reflecting surfaces: Physics, propagation, and pathloss modeling," *IEEE Wirel. Commun. Lett.*, vol. 9, no. 5, pp. 581–585, May 2020.